# Humic acid characteristics and effects on the reactivity of nano-scale zero-valent iron particles during nitrate reduction

Do-Gun Kim[a],*, Yu-Hoon Hwang[a], Hang-Sik Shin[a], Seok-Oh Ko[b]

[a]*Department of Civil and Environmental Engineering, Korea Advanced Institute of Science and Technology, 291, Gwahak-ro, Yuseong-gu, Daejeon 305-701, Republic of Korea*
*Tel. +82 42 350 3653; Fax +82 42 350 3610; email: dpblue@kaist.ac.kr*
[b]*Department of Civil Engineering, Kyung Hee University, 1732, Deokyoungdaero, Giheung-gu, Yongin 446-701, Republic of Korea*

### ABSTRACT

Humic acid (HA) comprises a significant fraction of natural organic matter (NOM), greatly influencing the performance of water and wastewater treatment processes. HA is expected to significantly affect the reactivity of nano-scale zero-valent iron (NZVI), which is receiving increasing attention due to its high reactivity. The effects of HA on nitrate reduction by NZVI were investigated to evaluate the potential of NZVI in practical applications. HA was characterized to identify the mechanism whereby HA affects. Nitrate reduction was enhanced at low HA concentration, but inhibited as HA concentration increased. HA decreased to reach a plateau and considerable amount of $Fe^{3+}$ was detected when HA was present in dissolved phase. The increase in the degree of condensation of HA was verified by UV–vis spectroscopy, fluorescence spectroscopy, and size exclusion chromatography. Fourier transform infrared spectra confirmed that the $Fe^{3+}$–HA complexes were formed in both the dissolved and solid fractions, without coexisting metal ions. The HA aggregation on NZVI and discrete HA macroaggregates were observed by transmission electron microscopy. The results suggest that HA induces complex effects on NZVI reactivity by improving iron dissolution, inhibiting readsorption of released iron, enhancing electron transfer, and inhibiting nitrate mass transfer via forming HA accumulation. It indicates that the clogging by aggregated NOM should be considered when NZVI is used for groundwater treatment or in combination with porous materials.

*Keywords:* Nano-scale zero valent iron; Nitrate; Humic acid; Aggregation; Iron–humic acid complex

## 1. Introduction

Nitrate generally exists in ground water, surface water, wastewater, wastewater treatment effluents, and membrane retentates. Nitrate is regulated in many countries because it causes blue baby syndrome, by decreasing the oxygen transport potential of blood when introduced into the human gut [1]. Recently, the chemical reduction of nitrate by metal nanoparticles, especially by nano-scale zero-valent iron (NZVI), has attracted a great attention due to high reaction rate and efficiency [2,3]. The reductive removal and adsorption of organic compounds, heavy metals, and disinfection by-products by NZVI has also been investigated [4–6].

Despite the great potential of NZVI, little attention has been paid to practical applications for water and wastewater treatment, although many

_____
*Corresponding author.

factors affecting NZVI reactivity, such as precursor concentration, particle size, pH, etc., have been studied [2–4,7]. Especially, the effects of coexisting pollutants, such as humic substances (HS), on nitrate removal by NZVI have seldom been investigated. HS, mainly humic acid (HA), are the most widely distributed type of organic matter, found in natural water, wastewater treatment effluent, and membrane retentates together with nitrate [8,9]. HS are heterogeneous mixtures of acidic, randomly polymerized, polydispersed, high-molecular-weight organic macromolecules, with widely differing chemical functional groups. HS play an important role in the fate, reactivity, and transport of pollutants by hydrophobic interactions, electrostatic interactions, hydrogen bonding, and coordinate bonding [10,11].

It is known that HA adversely affects the reactivity of heterogeneous catalysts, including NZVI. It was reported that the reactivity of Pd-Cu/$\gamma$-Al$_2$O$_3$ catalyst and photocatalyst was reduced by HA [12,13], and the NZVI toxicity to *Escherichia coli* and to *Bacillus subtilis* decreased in the presence of HA [14]. In addition, it was observed by the authors that nitrate removal by NZVI and Cu/NZVI was significantly inhibited when they were used for the treatment of reverse osmosis (R/O) membrane retentates, which have high dissolved organic content (not shown here). However, there are researches reporting on the different effects of HA. Doong and Lai [15] showed that perchloroethylene (PCE) reduction rate by Pd/zero-valent iron (ZVI) catalyst decreased as HA concentration increased. However, when HA adsorption onto Pd/ZVI catalyst was equilibrated after 24 h before PCE injection, PCE reduction rate increased at 20 mg L$^{-1}$ HA, decreased at 40 mg L$^{-1}$ HA, and again increased at 80 mg L$^{-1}$ HA. Feng et al. [16] reported that carbon tetrachloride reduction rate decreased as HA concentration increased from 0 to 1,000 mg L$^{-1}$; however, chloroform reduction rate increased in the presence of HA. Lee et al. [4] also observed that trichloroethylene (TCE) reduction by NZVI was significantly inhibited at 1–30 mg L$^{-1}$ HA, but it was enhanced at 50 mg L$^{-1}$ HA.

Although the effects of HA on pollutants removal kinetics and efficiency of NZVI or other catalysts have been studied, there are only limited studies about the interactions between HA and NZVI, which affect the reactivity of NZVI. It necessitates the investigation on the change of HA property during reaction between pollutants and NZVI. In this study, the effects of HA on nitrate reduction by NZVI were examined. The characteristics of HA were also investigate extensively by using UV–vis spectrophotometry, fluorescence spectrophotometry, size exclusion chromatography (SEC), Fourier transform infrared (FTIR) spectroscopy, and transmission electron microscopy (TEM).

## 2. Materials and methods

### 2.1. Materials

NZVI was prepared by chemical reduction of ferric ion [3]. Two hundred milliliters of 223.83 mM NaBH$_4$ solution were introduced dropwise at a flow rate of 5 mL min$^{-1}$ to 150 mL 59.69 mM Fe$^{3+}$ solution (FeCl$_3$·6H$_2$O). The NZVI particles were aged for 20 min, collected by filtration with a 0.45 μm cellulose acetate membrane filter, and washed with a large volume of deoxygenated deionized water (DDIW). The average diameter of NZVI was measured to be 16.70 nm using a laser scattering device (ZetaPlus, Brookhaven Instruments Corporation) and the Brunauer-Emmett-Teller surface area was found to be 17.62 ± 0.04 m$^2$ g$^{-1}$ (Sorptomatic 1990, Thermo Electron Corporation). Nitrate stock solution was prepared with KNO$_3$ and HA was prepared by purifying Aldrich HA powder by repeated pH adjustment, precipitation, and centrifugation [17]. The HA was freeze-dried and stored in a refrigerator at 4℃. All reagents were obtained from the Sigma-Aldrich.

### 2.2. Batch experiments

Batch experiments were conducted using a 1 L Schlenk flask at room temperature (20 ± 2℃) with continuous stirring. Nitrate and HA solution was prepared with DDIW and purged again with N$_2$ gas for 2 h before the injection of NZVI. The openings of the flask were sealed with stoppers and N$_2$ gas was bubbled during the reaction to prevent dissolution of ambient oxygen. Samples were taken periodically throughout the reaction period of 3 h and filtered with 0.45 μm cellulose acetate membrane filters for immediate analysis. The initial nitrate concentration and NZVI dose were 50 mg N L$^{-1}$ and 0.5 g L$^{-1}$, respectively. The initial HA concentration was varied from 6.25 to 100 mg L$^{-1}$, corresponding to 1.49–30.81 mg dissolved organic carbon (DOC) L$^{-1}$. To obtain the maximum HA adsorption capacity, DOC after a 3 h reaction at initial HA concentrations of 150 and 200 mg L$^{-1}$ (48.32 and 62.29 mg DOC L$^{-1}$) was additionally analyzed. A wide range of initial HA concentration was examined to investigate the effects of natural organic matter (NOM) when NZVI is applied to a variety of waters, i.e. natural water, wastewater treatment effluent, and R/O retentates [18,19], and to characterize the dissolved HA because high HA adsorption capacity of NZVI was reported [4]. All experiments were conducted in duplicate or triplicate.

*2.3. Analytical methods*

Concentrations of nitrate and nitrite were analyzed by ion chromatography (DX-120, Dionex). The samples for ammonia analysis were taken separately, acidified with 1 N HCl for short-term storage, and analyzed according to Standard Methods [20]. DOC in HA solutions was measured by a total organic carbon (TOC) analyzer (TOC-V CPH, Shimadzu). Total dissolved iron and ferrous iron were analyzed according to Standard Methods [20], and ferric iron concentration was obtained by subtracting ferrous iron concentration from total iron concentration.

UV–vis spectra, synchronous fluorescence (SF) spectra, and molecular weight distribution were obtained and analyzed for the dissolved HA fraction when the initial HA concentration was $100 \, mg \, L^{-1}$. UV–vis spectra were obtained with a UV–vis spectrophotometer (UV mini 1240, Shimadzu) at wavelengths from 800 to 200 nm. The absorbance at 254, 280, 465, 600, and 665 nm was recorded. SF spectra were collected using a spectrofluorometer (RF5301PC, Shimadzu), with a 10 mm cuvette at room temperature [21,22]. The excitation wavelengths in the SF spectra were 240–700 nm and the offsets between excitation and emission wavelengths ($\Delta\lambda$) were 21, 32, 44, 55, 66, and 77 nm. The effects of ferric iron on UV–vis spectra and SF spectra were not considered, because $Fe^{3+}$ concentration did not vary notably in the reaction period of 75–180 min. In addition, the intrinsic dimensionality of fluorophores is not affected by metal ions, although the intensity decreases [23].

Molecular weight distribution was analyzed with SEC using an absorbance detector (UV 730 D, Younglin), solvent degasser, valve module (SDV 30 Plus, Younglin), column oven (CTS 30, Younglin), auto sampler (MIDAS, Spark Holland), and a Protein Pak 125 column (Waters). The flow rate of the mobile phase was $0.8 \, mL \, min^{-1}$ and the pH of the mobile phase was maintained at 6.8 by adding phosphate (2 mM $NaH_2PO_4 \cdot H_2O$ and 2 mM $Na_2HPO_4$) to a 0.1 M NaCl solution. Sodium polystyrene sulfonate (PSS) standards of nominal molecular weights of 18, 8, 4.6, and 1.8 kDa were purchased from Polysciences, Inc. The four PSS samples and acetone (58 Da, HPLC grade, Aldrich) were used as standards. All standards and samples were measured at a detection wavelength of 254 nm. A calibration curve was established with the linear relationship between the retention time of corresponding peaks and the logarithm of actual weight-average molecular weight ($MW_w$). The $MW_w$ and number average molecular weight ($MW_n$) were determined by Eqs. (1) and (2):

$$MW_w = \frac{\sum_{i=1}^{N} (h_i MW_i)}{\sum_{i=1}^{N} (h_i)} \tag{1}$$

$$MW_n = \frac{\sum_{i=1}^{N} (h_i)}{\sum_{i=1}^{N} (h_i / MW_i)} \tag{2}$$

where $h_i$ and $MW_i$ represent signal height and molecular weight, respectively [24].

The solid phase mixture of NZVI and HA aggregates was collected by 0.45 μm cellulose acetate filter after a 3 h reaction, when initial HA concentration was 100 and $150 \, mg \, L^{-1}$. The solid phase mixture and the filtrate were freeze-dried separately for FTIR analysis of the solid phase and the dissolved phase, respectively. The FTIR spectra were obtained with KBr disks made of the sample containing 1 mg DOC and 200 mg FTIR grade KBr (Sigma-Aldrich), by an FTIR spectrometer (Spectrum One System, Perkin Elmer). The amount of the mixture was calculated based on the removed DOC and NZVI concentration. The solid phase mixture was further investigated using TEM (Tecnai F20, Philips) with energy dispersive X-ray (EDX) analysis.

## 3. Results and discussion

### 3.1. Effect of HA on nitrate removal and ammonia generation

The concentrations of nitrate and ammonia are illustrated in Fig. 1, while the concentrations of DOC and $Fe^{3+}$ concentration are provided in Fig. 2. Nitrate removal and ammonia generation were promoted when the initial HA concentrations were 6.25 and $12.5 \, mg \, L^{-1}$, but were inhibited at higher than $50 \, mg \, L^{-1}$ HA (Fig. 1). DOC was almost completely removed within 30 min at initial HA concentrations of $6.25–50 \, mg \, L^{-1}$ and trace amounts of organic carbon were detected (Fig. 2). The maximum adsorption amount at $100–200 \, mg \, L^{-1}$ HA was $37.20 \pm 1.51 \, mg$ DOC g $NZVI^{-1}$, which corresponds to $113.074 \pm 2.327 \, mg$ HA g $NZVI^{-1}$. The results demonstrate that nitrate reduction was enhanced at low HA concentration, but the enhancement of the reaction turned into inhibition as the HA accumulation on the NZVI surface increased.

Meanwhile, two distinct regions were observed in the profiles of nitrate and ammonia at $12.5–100 \, mg \, L^{-1}$ HA. The first region (0–30 min of reaction time) corresponds to the period before the DOC reached an equilibrium concentration, i.e. when HA accumulation on NZVI was in progress. The second region (60–180 min
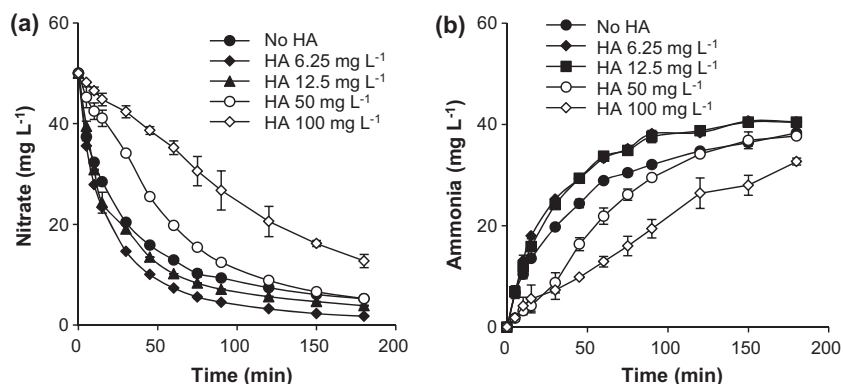
Fig. 1. Concentrations of nitrate (a) and ammonia (b) during nitrate reduction by NZVI at various initial HA concentrations.
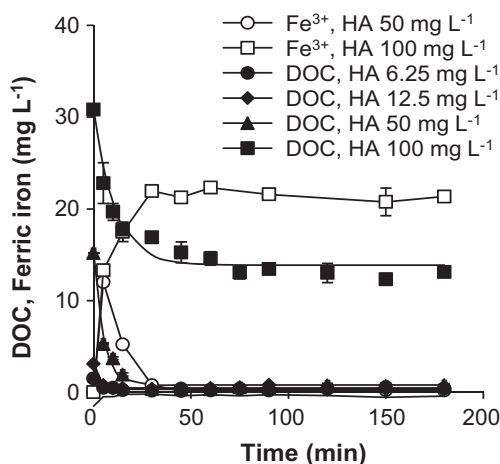


Fig. 2. Concentrations of DOC and ferric iron during nitrate reduction by NZVI at various initial HA concentrations.

of reaction time) corresponds to the period when HA mass on NZVI was constant (Fig. 2). A similar nitrate profile has also been observed by Hwang et al. [25], when an organic buffer 4-(2-hydroxyethyl)-1-piperazineethanesulfonic acid (HEPES) was used for pH buffer during nitrate reduction by NZVI. The variation of nitrate removal rate during the first region may be attributed to the enhanced electron transfer by HA at the iron–water interface and by the competition of nitrate with HA. The NOM and hydroquinone/quinine type couples are efficient electron transfer mediators between the $Fe^0$ and target compounds [15,26]. On the other hand, nitrate is in competition with organic components and other anions, i.e. phosphate and sulfate [27]. Nitrate removal rate in the second region was lower than the first region because HA accumulation on NZVI surface was at the maximum for each batch experiment. It indicates nitrate mass transfer can be

inhibited by the accumulated HA or other organic compounds on NZVI. It was also reported that the reactivity of microscale ZVI was affected by the amount of HEPES added for pH control [28].

### 3.2. HA removal and iron release

As shown in Fig. 2, DOC reached equilibrium during the 3 h reaction. The adsorption kinetic behavior was fitted to the pseudo first-order adsorption kinetic equation. The pseudo first-order adsorption rate constants for 6.25, 12.5, 50, and $100 \, mg \, L^{-1}$ HA were 0.402, 0.400, 0.196, and $0.091 \, min^{-1}$, respectively. The rate constant decreased significantly as the initial HA concentration increased to higher than $50 \, mg \, L^{-1}$. Fig. 2 also shows that $Fe^{3+}$ is present only when HA is present in dissolved phase, i.e. when initial HA concentration was 50 or $100 \, mg \, L^{-1}$. $Fe^{3+}$ concentration was negligible throughout the reaction period when initial HA concentration was $0–12.5 \, mg \, L^{-1}$. Ferric iron was dominant for all samples ($98.60 \pm 2.07 \, \%$ of total dissolved iron).

Based on the results in Fig. 2, it is regarded that the removal of dissolved HA is not only by the adsorption but also by aggregation induced by the complexation of HA with $Fe^{3+}$. At initial HA concentration of $50 \, mg \, L^{-1}$, $Fe^{3+}$ concentration was at its maximum of $12.00 \, mg \, L^{-1}$ at 5 min. Then it decreased rapidly to be negligible after 30 min, when HA concentration also became negligible. This implies that $Fe^{3+}$ formed complexes with HA molecules so that $Fe^{3+}$ and HA were removed simultaneously from the dissolved phase. The aggregation and adsorption of NOM onto solid surfaces can be promoted by charge neutralization, coprecipitation, and the binding of multivalent cations, such as $Fe^{3+}$ and $Ca^{2+}$. The binding of metal ions with functional groups of NOM results in the formation of

a more condensed NOM structure [29,30]. In addition, the iron release from $Fe^0$ can be enhanced in the presence of HA by the ligand-promoted iron dissolution [31] and it is known that $Fe^{2+}$, released as the result of the reduction of nitrate or nitrite, is subsequently oxidized to $Fe^{3+}$ [32]. Liu et al. [27] reported that, in a system of $20 \, mg \, L^{-1} \, Cr^{6+}$, $0.8 \, mM \, Ca^{2+}$ or $Mg^{2+}$, $10.53 \, g \, L^{-1}$ ZVI, and $20 \, mg \, L^{-1}$ HA as DOC, dissolved iron concentration increased to $5–10 \, mg \, L^{-1}$ when DOC decrease was not significant. Then both the iron and DOC concentrations decreased rapidly possibly because of the Fe–humate complexes formation encouraged by coexisting $Ca^{2+}$ or $Mg^{2+}$. However, the results presented in Fig. 2 indicate that iron dissolution and $Fe^{3+}$–HA complex formation are promoted in the presence of NZVI, without coexsting metal ions. It also implies that the pores in soil or subsequent sand filters or membranes can be blocked when NZVI is used for the treatment of water with high HA content.

Meanwhile, at $100 \, mg \, L^{-1}$ HA, $Fe^{3+}$ concentration increased drastically in the early reaction period of 0–45 min and was maintained at $21.45 \pm 0.57 \, mg \, L^{-1}$ during 45–180 min (Fig. 2). It strongly indicates that the $Fe^{3+}$–HA complexes exist not only in the solid phase, either on the NZVI surface or suspended in solution, but also in the dissolved phase. The existence of $Fe^{3+}$ in dissolved phase at $50–100 \, mg \, L^{-1}$ HA also implies that the readsorption of released iron and the subsequent formation of iron hydroxy oxide shell on NZVI surface [32] can be inhibited by HA. Thus nitrate reduction can be promoted when HA concentration is lower, so that the inhibition of nitrate mass transfer was not inhibited by the significant HA accumulation on NZVI (Fig. 1).

### 3.3. UV–vis spectroscopy of dissolved HA fraction after reaction with NZVI

The results of UV–vis spectroscopy at $100 \, mg \, L^{-1}$ HA are presented in Fig. 3. UV–vis absorbance increased at all wavelengths throughout the reaction period (Fig. 3(a)). The DOC specific UV–vis absorbance such as the ratio between UV–vis absorbance at 254 nm and DOC ($SUVA_{254}$), between UV–vis absorbance at 280 nm and DOC ($SUVA_{280}$), and between UV–vis absorbance at 600 nm and DOC ($SVISA_{600}$),
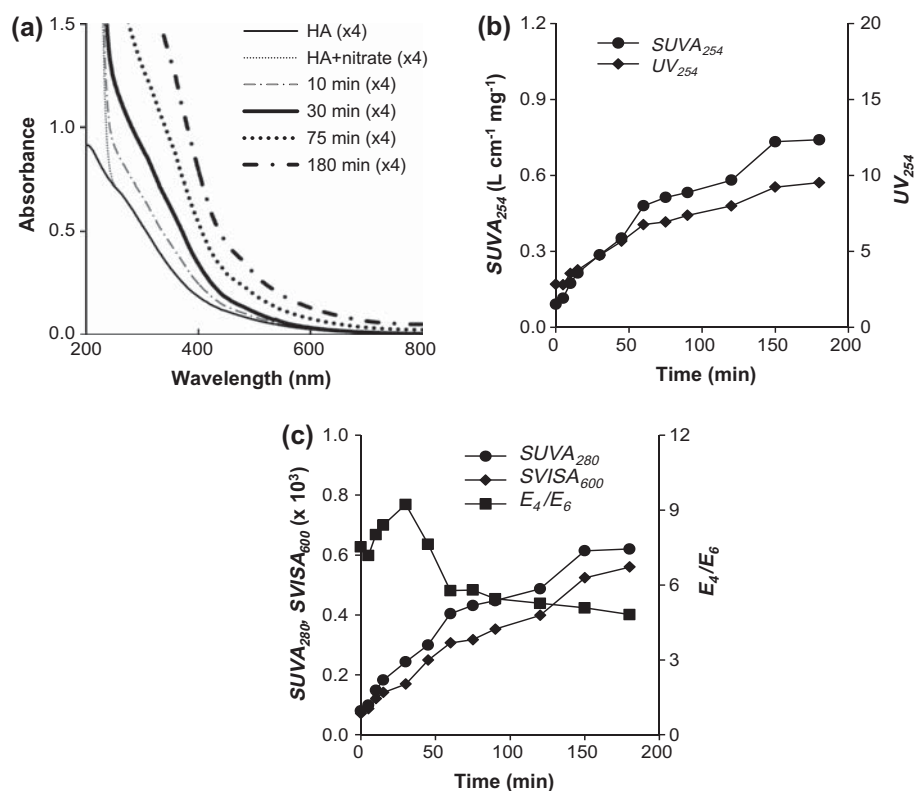
Fig. 3. UV–vis spectra (a), $SUVA_{254}$ and $UV_{254}$ (b), and $SUVA_{280}$, $SVISA_{600}$, and $E_4/E_6$ (c) during nitrate reduction by NZVI at initial HA concentration of $100 \, mg \, L^{-1}$.

was investigated. The absorbance at 254 nm ($UV_{254}$) and the ratio of UV–vis absorbance at 465 nm to 665 nm ($E_4/E_6$) were also investigated. $UV_{254}$ and $SUVA_{254}$ are known to be proportional to apparent molecular weight and aromaticity because aromatic rings and conjugated double bonds absorb UV at 254 nm [24,32]. $SUVA_{280}$ represents the total aromaticity, because the $\pi$–$\pi^*$ electron transition for phenolic arenes, benzoic acids, aniline derivatives, polyenes, and polycyclic aromatic hydrocarbons occur at the 270–280 nm. $SVISA_{600}$ is positively correlated with the degree of aromaticity of HS of aquatic origin [33]. $E_4/E_6$ is inversely proportional to the molecular size of dissolved organic matter and the degree of condensation of aromatic groups [23].

$UV_{254}$ and $SUVA_{254}$ increased continuously (Fig. 3 (b)) although DOC decreased (Fig. 2). $UV_{254}$ has been adopted as the indicator of HA concentration in an aqueous solution, even after undergoing a reaction in the presence of NZVI [4,34]. However, $UV_{254}$ did not show a correlation with DOC in this study possibly because of a significant change in HA structure. $SUVA_{280}$ and $SVISA_{600}$ also increased, while $E_4/E_6$ decreased after 45 min (Fig. 3(c)). The increase of $SUVA_{254}$, $SUVA_{280}$, and $SVISA_{600}$ (Fig. 3(b)) and the decrease of $E_4/E_6$ after 45 min (Fig. 3(c)) indicate the increase of aromaticity and of the degree of condensation of HA during reaction with NZVI. The increase of $E_4/E_6$ in 0–30 min might be due to the increase of $Fe^{3+}$ (Fig. 2). The condensation of HA molecules can occur by oxidative coupling reaction [35]. However, under the reductive condition in this study, the increase of the degree of condensation of HA would be the result of the complexation of HA with $Fe^{3+}$ released as a result of nitrate reduction, as indicated in Fig. 2 [17,29].

### 3.4. Fluorescence spectroscopy of dissolved HA fraction after reaction with NZVI

The SF spectra at 100 mg L$^{-1}$ HA show a continuous shift of a peak at 450–600 nm to longer emission wavelength, during reaction with NZVI (Fig. 4(a)). The "red shift" indicates the increase in higher molecular weight fractions of HA, which is consistent with the results of UV–vis spectroscopy (Fig. 3). The peaks at higher emission wavelengths generally indicate an increase in aromatic structure of a higher degree of condensation with more aromatic rings and the increasing hydrophobicity [36,37]. The increase of the degree of conjugation could be more significant than observed in Fig. 4, because aromatic and/or polyphenolic contents with mostly high molecular weight do not show fluorescence intensity around 550 nm in SF spectra [33].

Fig. 4(b) illustrates the SF spectra at 50 mg L$^{-1}$ HA. The "red shift" is also observed after 10 min, but the fluorescence intensity at 450–600 nm decreased rapidly as DOC decreased. However, the relative intensity in the regions less than 400 nm increased after 30 min, when DOC decreased to $0.73 \pm 0.15$ mg L$^{-1}$. The increase of peak intensity at lower emission wavelengths is associated with the increase of lower molecular weight compounds such as alcohols, aldehydes, ketones, and carboxylic acids [23,38]. It indicates that higher molecular weight fraction of HA was precipitated or adsorbed on NZVI prior to the lower molecular weight fraction.

### 3.5. SEC of dissolved HA fraction

The increase of the relatively high-molecular-weight domain in SEC chromatographs are observed when the initial HA concentration was 100 mg L$^{-1}$ (Fig. 5(a)). The fact that $MW_w$ and $MW_n$ increase
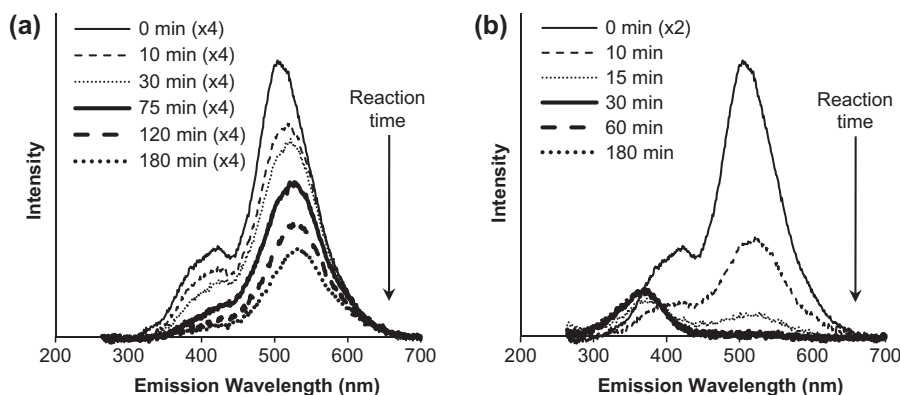


Fig. 4. SF spectra at $\Delta\lambda = 44$ nm during nitrate reduction by NZVI at initial HA concentration of 100 mg L$^{-1}$ (a) and of 50 mg L$^{-1}$ (b).

similarly as time indicates the aggregation formation of HA (Fig. 5(b)). Polydispersity, the ratio of $MW_w$ to $MW_n$, increased as the reaction started. It implies that the structure of the dissolved organic fraction become less rigid and has wider size distribution [10,38]. Meanwhile, when the initial HA concentration was $50\,mg\,L^{-1}$, the peak in SEC chromatograph was also shifted to a higher average molecular weight domain in 5–15 min, indicating that the higher molecular weight fraction increased. However, no signal was detected after 30 min because DOC decreased to a negligible value (not shown here).

The results in Fig. 5 confirm the formation of the condensed HA structure by the reaction with NZVI. The increase of the degree of conjugation of HA is known to be the result of the oxidative coupling of phenolic monomers, such as catechol and pyrogallol, in the presence of redox active oxides or oxidative enzymes, such as birnessite or horseradish peroxidase [39,40]. However, the formation of radial coupling products of TCE in anoxic condition in the presence of NZVI was also reported [41].

### 3.6. FTIR spectra and TEM

The FTIR spectra of HA showed typical bands for HA as presented in Fig. 6(a) [8]. After 3 h reaction of $100\,mg\,L^{-1}$ HA, $50\,mg\,L^{-1}$ nitrate, and $0.5\,g\,L^{-1}$ NZVI, there were clear changes in the characteristic bands (Fig. 6(b) and (c)). The intensity of the bands assigned to O–H stretchings ($3,400$–$3,300\,cm^{-1}$) and to aromatic C=C and COO– symmetric stretching ($1,600$–$1,575$ $cm^{-1}$) decreased significantly. The bands assigned to aliphatic C–H, C–$H_2$, and C–$H_3$ stretching ($2,940$–$2,900\,cm^{-1}$) and to carboxylate ion stretching ($2,870\,cm^{-1}$) disappeared both from the solid fraction
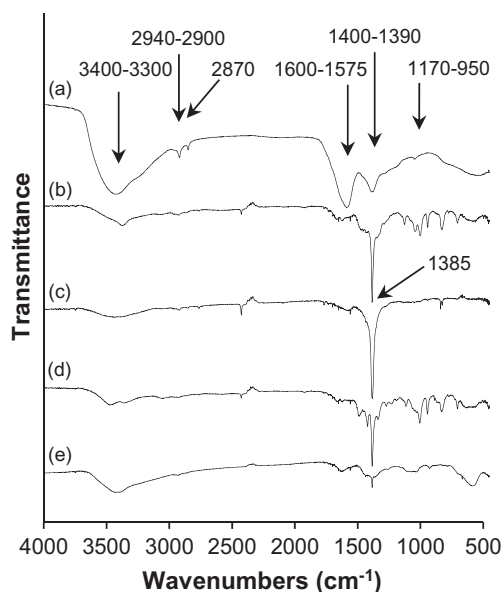


Fig. 6. FTIR spectra of the HA (a); of the solid fraction (b), of the dissolved organic fraction (c) after a 3 h reaction at initial HA concentration of $100\,mg\,L^{-1}$; of the solid fraction (d), and the dissolved organic fraction (e) after a 3 h reaction at initial HA concentration of $150\,mg\,L^{-1}$.

and dissolved fraction. Instead, a strong peak at $1,835\,cm^{-1}$, assigned to the –COO–metal stretching [42], appeared in the spectra of both the solid fraction and the dissolved fraction (Fig. 6(b) and (c)). The band assigned to phenolic OH, C–H deformation of $CH_2$ and $CH_3$ groups, and COO– antisymmetric stretching ($1,400$–$1,390\,cm^{-1}$) was overlapped by the band at $1,385\,cm^{-1}$.

The FTIR spectra presented in Fig. 6(b) and (c) and the $Fe^{3+}$ concentration presented in Fig. 2 confirm that $Fe^{3+}$–HA complexes can be formed by NZVI in the
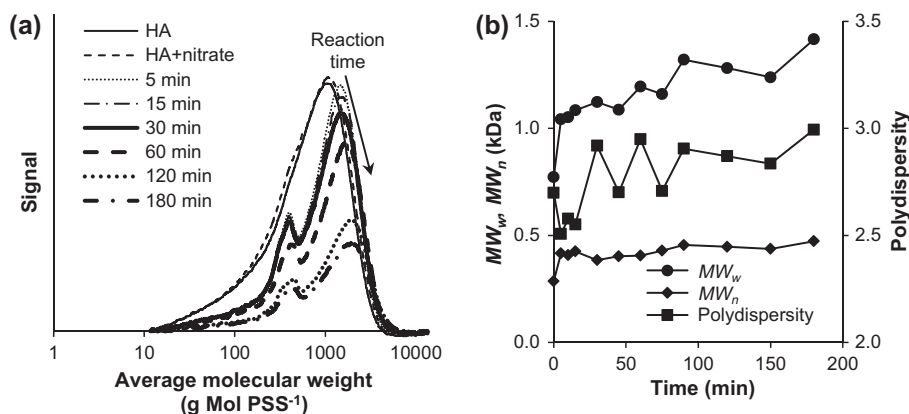


Fig. 5. Molecular weight distribution (a) and average molecular weight and polydispersity (b) during reaction with NZVI, at initial HA concentration of $100\,mg\,L^{-1}$.
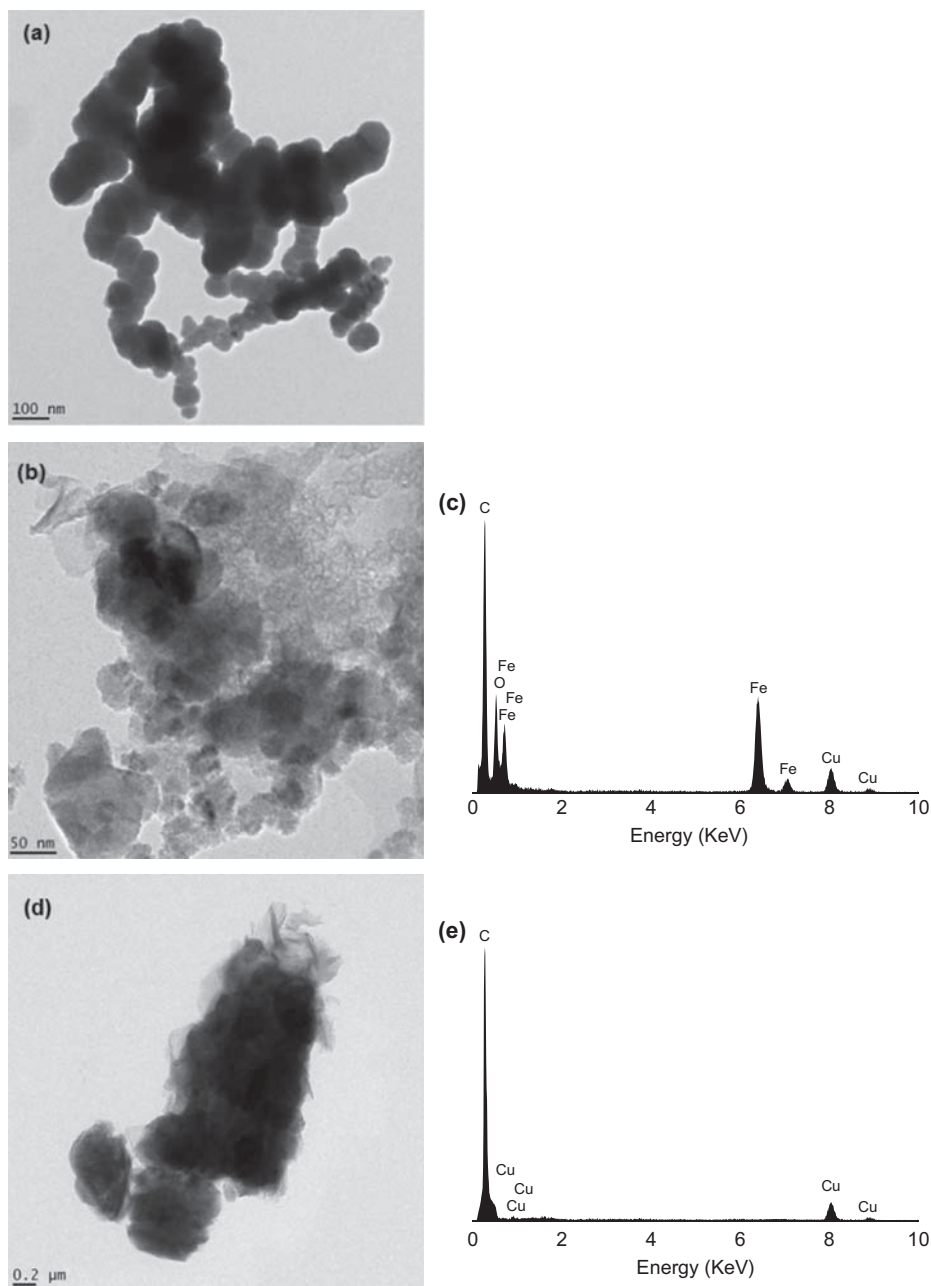
Fig. 7. TEM image of NZVI before reaction (a); TEM image of solid fraction collected after 3 h reaction with initial HA concentration of $100 \, mg \, L^{-1}$ (b); and EDX analysis of (b) (c); TEM image of organic aggregates observed in the solid fraction collected after 3 h reaction at initial HA concentration of $100 \, mg \, L^{-1}$ (d); and EDX analysis of (d) (e).

absence of coexisting metal ions, such as $Ca^{2+}$ and $Mg^{2+}$. Tsang et al. [42] showed the increase of average molecular weight of HA's of various origins, including purified Aldrich HA, by reaction with ZVI in a background solution of 5 mM NaCl and 0.8 mM $CaCl_2$. However, it was also shown that HA aggregation was negligible without the background ions [42].

Similar FTIR spectra were obtained when the initial HA concentration was 100 and $150 \, mg \, L^{-1}$ (Fig. 6

(b) and (d)) for solid phase. However, at $150 \, mg \, L^{-1}$ HA, the band intensity at $1,385 \, cm^{-1}$ for dissolved fraction was not as strong as observed at $100 \, mg \, L^{-1}$ HA (Fig. 6(e)). It indicates that the fraction of $Fe^{3+}$–HA complexes from the total dissolved HA is lower because of the existence of more unreacted HA at higher initial HA concentration. Meanwhile, the band at $1,170–950 \, cm^{-1}$ is observed only for the solid fraction (Fig. 6(b) and (d)), implying that carbohydrates

and polysaccharide-like substances, which are high-molecular-weight fraction of HA and cause fouling of UF membranes [43], are readily adsorbed onto NZVI or aggregated.

TEM image of fresh NZVI is presented in Fig. 7(a). The mixture of organic aggregates and NZVI was observed by TEM and EDX analysis as shown in Fig. 7(b) and (c). It verifies that the decrease of DOC during the reaction was attributed to both adsorption onto NZVI surfaces and aggregation of HA. In addition, discrete organic aggregates, not attached to NZVI surface, were also observed (Fig. 7(d) and (e)). It is regarded that the organic aggregates are formed around NZVI and then separated by agitation because $Fe^{3+}$–HA complexes can promote the HA aggregation and serve as the nuclei for macroaggregate formation [44].

## 4. Conclusions

In this study, effects of HA on nitrate reduction by NZVI were evaluated and the properties of HA were investigated extensively to understand the affecting mechanism by HA. Nitrate reduction by NZVI was enhanced with $12.5\,mg\,L^{-1}$ HA or less, but it was inhibited as initial HA concentration increased. HA decreased to reach an equilibrium concentration and significant amount of $Fe^{3+}$ was observed at high initial HA concentration. The formation of a more condensed HA structure in dissolved HA fraction was verified by UV–vis spectra, SF spectra, and SEC chromatography. TEM analysis of the solid fraction after a 3 h reaction confirmed the HA aggregation around NZVI and HA aggregates, which exist out of NZVI surface. The formation of the complexes of $Fe^{3+}$ and the COOH group of HA was verified by FTIR spectra in both the dissolved phase and solid phase. It indicates that $Fe^{3+}$–HA complexation is greatly promoted by NZVI, even in the absence of coexisting metal ions. It also indicates that the $Fe^{3+}$–HA complex formation contributes to the HA removal from dissolved phase and to the decrease of readsorption of released iron and the formation of iron hydroxy oxide shell.

According to the results presented, it can be concluded that HA induces complex effects on NZVI by enhancing of electron transfer, competing with reactants, promoting iron dissolution, inhibiting iron hydroxy oxide shell formation, being accumulated on NZVI surface via forming aggregates encouraged by complexation with $Fe^{3+}$, and inhibiting mass transfer of reactants to NZVI surface. Therefore, it is suggested that the organic compounds should be removed to a certain level, when NZVI is applied for water or wastewater with high organic content, because it can cause the decrease of NZVI reactivity and the clogging of membranes or filters.

## References

[1] A. Kapoor, T. Viraraghavan, Nitrate removal from drinking water-review, J. Environ. Eng. (ASCE) 123 (1997) 371–380.
[2] Y.H. Liou, S.-L. Lo, C.-J. Lin, W.H. Kuan, S.C. Weng, Chemical reduction of an unbuffered nitrate solution using catalyzed and uncatalyzed nanoscale iron particles, J. Hazard. Mater. 127 (2005) 102–110.
[3] G.C.C. Yang, H.-L. Lee, Chemical reduction of nitrate by nanosized iron: Kinetics and pathways, Water Res. 39 (2005) 884–894.
[4] Y.-C. Lee, C.-W. Kim, J.-Y. Lee, H.-J. Shin, J.-W. Yang, Characterization of nanoscale zero valent iron modified by non-ionic surfactant for trichloroethylene removal in the presence of humic acid: A research note, Desalin. Water Treat. 10 (2009) 33–38.
[5] Y.C. Sharma, V. Srivastava, V.K. Singh, S.N. Kaul, C.H. Weng, Nano-adsorbents for the removal of metallic pollutants from water and wastewater, Environ. Technol. 30 (2009) 583–609.
[6] Y. Zhang, Y. Lia, X. Zheng, Removal of atrazine by nanoscale zero valent iron supported on organobentonite, Sci. Tot. Environ. 409 (2011) 625–630.
[7] Y.H. Liou, S.-L. Lo, W.H. Kuan, C.-J. Lin, S.C. Weng, Effect of precursor concentration on the characteristics of nanoscale zerovalent iron and its reactivity of nitrate, Water Res. 40 (2006) 2485–2492.
[8] F.J. Stevenson, Humus Chemistry: Genesis, Composition, Reactions, John Wiley and Sons, New York, NY, 1982.
[9] S. Van Geluwe, L. Braeken, C. Vinckier, B. Van der Bruggen, Ozonation and perozonation of humic acids in nanofiltration concentrates, Desalin. Water Treat. 6 (2009) 217–221.
[10] Y.-P. Chin, G. Aiken, E. O'Loughlin, Molecular weight, polydispersity, and spectroscopic properties of aquatic humic substances, Environ. Sci. Technol. 28 (1994) 1853–1858.
[11] K. Nakashima, S. Xing, Y. Gong, T. Miyajima, Characterization of humic acids by two-dimensional correlation fluorescence spectroscopy, J. Mol. Struc. 883–884 (2008) 155–159.
[12] B.P. Chaplin, E. Roundy, K.A. Guy, J.R. Shapley, C.J. Werth, Effects of natural water ions and humic acid on catalytic nitrate reduction kinetics using an alumina supported Pd-Cu catalyst, Environ. Sci. Technol. 40 (2006) 3075–3081.
[13] J. Marugáán, R. van Grieken, C. Pablos, Kinetics and influence of water composition on photocatalytic disinfection and photocatalytic oxidation of pollutants, Environ. Technol. 31 (2010) 1435–1440.
[14] J. Chen, Z. Xiu, G.V. Lowry, P.J.J. Alvarez, Effect of natural organic matter on toxicity and reactivity of nano-scale zerovalent iron, Water Res. 45 (2011) 1995–2001.
[15] R.-A. Doong, Y.-J. Lai, Dechlorination of tetrachloroethylene by palladized iron in the presence of humic acid, Water Res. 39 (2005) 2309–2318.
[16] J. Feng, B.-W. Zhu, T.-T. Lim, Reduction of chlorinated methanes with nano-scale Fe particles: Effects of amphiphiles on the dechlorination reaction and two-parameter regression for kinetic prediction, Chemosphere 73 (2008) 1817–1823.
[17] J. Hur, M.A. Schlautman, Using selected operational descriptors to examine the heterogeneity within a bulk humic substance, Environ. Sci. Technol. 5 (2003) 880–887.

[18] P. Westerhoff, H. Moon, D. Minakata, J. Crittenden, Oxidation of organics in retentates from reverse osmosis wastewater reuse facilities, Water Res. 43 (2009) 3992–3998.

[19] M.C. Brum, J.F. Oliveira, Removal of humic acid from water by precipitate flotation using cationic surfactants, Miner. Eng. 20 (2007) 945–949.

[20] American Public Health Association (APHA), Standard Methods for the Examination of Water and Wastewater, 20th ed., APHA, AWWA, WPCF, Washington, DC, 1998.

[21] J. Świetlik, E. Sikorska, Application of fluorescence spectroscopy in the studies of natural organic matter fractions reactivity with chlorine dioxide and ozone, Water Res. 38 (2004) 3791–3799.

[22] T. Zhang, J. Lu, J. Ma, Z. Qiang, Fluorescence spectroscopic characterization of DOM fractions isolated from a filtered river water after ozonation and catalytic ozonation, Chemosphere 71 (2008) 911–921.

[23] M.C.G. Antunes, C.C.C. Pereira, J.C.G.E. da Silva, MCR of the quenching of the EEM of fluorescence of dissolved organic matter by metal ions, Anal. Chim. Acta 595 (2007) 9–18.

[24] J. Hur, M.A. Schlautman, Evaluating spectroscopic and chromatographic techniques to resolve dissolved organic matter via end member mixing analysis, Chemosphere 63 (2006) 387–402.

[25] Y.H. Hwang, D.G. Kim, Y.T. Ahn, C.M. Moon, H.S. Shin, Fate of nitrogen species in nitrate reduction by nanoscale zero valent iron and characterization of the reaction kinetics, Water Sci. Technol. 61 (2010) 705–712.

[26] R.P. Schwarzenbach, R. Stierli, K. Lanz, J. Zeyer, Quinone and iron porphyrin mediated reduction of nitroaromatic compounds in homogeneous aqueous solution, Environ. Sci. Technol. 24 (1994) 1566–1574.

[27] T. Liu, D.C. Tsang, I.M. Lo, Chromium(VI) reduction kinetics by zero-valent iron in moderately hard water with humic acid: Iron dissolution and humic acid adsorption, Environ. Sci. Technol. 42 (2008) 2092–2098.

[28] L.L. Zawaideh, T.C. Zhang, The effects of pH and addition of an organic buffer (HEPES) on nitrate transformation in $Fe^0$-water systems, Water Sci. Technol. 38 (1998) 107–115.

[29] A.-V. Jung, V. Chanudet, J. Ghanbaja, B.S. Lartiges, J.-L. Bersillon, Coagulation of humic substances and dissolved organic matter with a ferric salt: An electron energy loss spectroscopy investigation, Water Res. 39 (2005) 3849–3862.

[30] K.-S. Lin, N.-B. Chang, T.-D. Chuang, Fine structure characterization of zero-valent iron nanoparticles for decontamination of nitrites and nitrates in wastewater and groundwater, Sci. Technol. Adv. Mater. 169 (2008) 23–31.

[31] P.F.A.M. Romkens, J. Dolfing, Effect of Ca on the solubility and molecular size distribution of DOC and Cu binding in soil solution samples, Environ. Sci. Technol. 32 (1998) 363–369.

[32] W. Stumm, Reactivity at the mineral-water interface: Dissolution and inhibition, Colloid Surf. A 120 (1997) 143–166.

[33] C.S. Uyguner, M. Bekbolet, Evaluation of humic acid photocatalytic degradation by UV–vis and fluorescence spectroscopy, Catal. Today 101 (2005) 267–274.

[34] A.M. Giasuddin, S.R. Kanel, H.C. Choi, Adsorption of humic acid onto nanoscale zerovalent iron and its effect on arsenic removal, Environ. Sci. Technol. 41 (2007) 2022–2027.

[35] D. Šmejkalovǎ, P. Conte, A. Piccolo, Structural characterization of isomeric dimers from the oxidative oligomerization of catechol with a biomimetic catalyst, Biomacromolecules 8 (2007) 737–743.

[36] T.M. Miano, N. Senesi, Synchronous excitation fluorescence spectroscopy applied to soil humic substances chemistry, Sci. Tot. Environ. 117 (1992) 41–51.

[37] N. Hudson, A. Baker, D. Reynolds, Fluorescence analysis of dissolved organic matter in natural, waste and polluted waters-A review, River Res. Appl. 23 (2007) 631–649.

[38] E.J. O'Loughlin, Y.-P. Chin, Quantification and characterization of dissolved organic carbon and iron in sedimentary porewater from Green Bay, WI, USA, Biogeochemistry 71 (2004) 371–386.

[39] D. Šmejkalovǎ, A. Piccolo, Rates of oxidative coupling of humic phenolic monomers catalyzed by a biomimetic iron-porphyrin, Environ. Sci. Technol. 40 (2006) 1644–1649.

[40] A.G. Hardie, J.J. Dynes, L.M. Kozak, P.M. Huang, Influence of polyphenols on the integrated polyphenol-Maillard reaction humification pathway as catalyzed by birnessite, AES 1 (2007) 91–110.

[41] Y. Liu, S.A. Majetich, R.D. Tilton, D.S. Sholl, G.V. Lowry, TCE dechlorination rates, pathways, and efficiency of nanoscale iron particles with different properties, Environ. Sci. Technol. 39 (2005) 1338–1345.

[42] D.C.W. Tsang, N.J.D. Graham, I.M.C. Lo, Humic acid aggregation in zero-valent iron systems and its effects on trichloroethylene removal, Chemosphere 75 (2009) 1338–1343.

[43] S.V. Geluwe, L. Braeken, C. Vinckier, B. Van der Bruggen, Ozonation and perozonation of humic acids in nanofiltration concentrates, Desalin. Water Treat. 6 (2009) 217–221.

[44] J. Haberkamp, M. Ernst, H. Paar, D. Pallischeck, G. Amy, M. Jekel, Impact of organic fractions identified by SEC and fluorescence EEM on the hydraulic reversibility of ultrafiltration membrane fouling by secondary effluents, Desalin. Water Treat. 29 (2011) 73–86.